CHARACTERIZATION OF THE ORTHOTROPIC ELASTIC TENSOR OF COMPOSITES USING FULL-FIELD LAMB WAVES

Conference Paper · December 2020

DOI: 10.48465/fa.2020.0909

7 authors, including:

Adil Han Orta
KU Leuven
11 PUBLICATIONS **28** CITATIONS
SEE PROFILE

Joost Segers
Ghent University
38 PUBLICATIONS **143** CITATIONS
SEE PROFILE

Jeroen Vandendriessche
Ghent University
1 PUBLICATION **0** CITATIONS
SEE PROFILE

Wim Van Paepegem
Ghent University
578 PUBLICATIONS **6,866** CITATIONS
SEE PROFILE

CHARACTERIZATION OF THE ORTHOTROPIC ELASTIC TENSOR OF COMPOSITES USING FULL-FIELD LAMB WAVES

Adil Han Orta[1] **Joost Segers**[2] **Jeroen Vandendriessche**[2]
Nicolaas Bernardus Roozen[3] **Wim Van Paepegem**[2] **Mathias Kersemans**[2]
Koen Van Den Abeele[1]

[1] Wave Propagation and Signal Processing, Department of Physics,
KU Leuven – Kulak, Belgium

[2] Mechanics of Materials and Structures, Department of Materials,
Textiles and Chemical Engineering, Ghent University, Belgium

[3] KU Leuven, Laboratory of Acoustics, Department of Physics,
Celestijnenlaan 200D, Leuven, Belgium

adilhan.orta@kuleuven.be

ABSTRACT

In structural design and structural health monitoring (SHM), characterization of the elastic stiffness tensor of materials is fundamental. However, due to anisotropy and matrix-fiber interactions in commonly used composite materials, the accurate reconstruction of these stiffness coefficients becomes a complex problem. In the present study, an inversion procedure is proposed based on 3D component Lamb wave phase velocity matching to identify the stiffness parameters of orthotropic composite plates. Experiments have been performed on an aluminum and a composite plate using either broadband (50-200 kHz) or narrowband signals (5-cycle Hanning-filtered tone burst at 240 kHz) generated by a piezoelectric actuator. A 3D Infrared Scanning Laser Doppler Vibrometer is used for in- and out-of-plane velocity measurements on the surface of the plate. These measurement data are converted into frequency-wavenumber space by way of 3D Fourier transform, and dispersion curves are extracted in 3D. For the forward model, the third order shear deformation theory (3SDT) is used and embedded in an inversion algorithm. The 3SDT model's accuracy at low frequencies and its computational efficiency allows to calculate truthful 3D dispersion curves of layered composite in less than a second, which is crucial for the inversion procedure. The expected stiffness parameters are calculated by minimizing the error between the first three measured and calculated lamb wave modes (A_0, S_0 and SH_0). As part of the study, different heuristic optimization algorithms such as surrogate optimization, particle swarm, genetic algorithm and simulated annealing have been considered, and their performance has been evaluated in terms of accuracy and efficiency. The reconstructed stiffness properties for an Aluminum sample and a quasi-isotropic composite plate with quasi-isotropic stacking sequence are compared with values from the literature, showing good agreement, with a mean difference around 3.1% for all 9 stiffness parameters.

1. INTRODUCTION

On one hand, characterization of the visco-elastic stiffness tensor of composites is fundamental in structural design applications. In addition, gradual material degradation, for instance due to cyclic thermal or stress exposure, or an abrupt impact might also change the visco-elastic moduli of the materials. Therefore, methods that are able to perform a timely and accurate characterization of materials are essential in nondestructive evaluation (NDE), structural health monitoring (SHM) and Noise Vibration and Harshness (NVH) and are crucial for instance for applications in automotive and aerospace industries.

In the past few decades, different inversion procedures have been developed to identify the elastic constants of materials. Destructive techniques such as tensile, compression and shear tests can provide only a few of the elastic moduli. The use of non-destructive techniques based on ultrasonic waves has many advantages compared to conventional methods [1]. Among the ultrasonic methods, wave propagation based characterization employing bulk waves [2–7] or guided waves [8–11] is well recognized. In both methods, identification of the medium's elasticity is mainly expressed by phase velocity measurements of a propagating ultrasonic wave inside the material [12]. By applying an accurate forward wave propagation model within a suitable inversion procedure, all (or a subset of the) stiffness constants can be inferred.

Despite the fact that bulk wave models are extremely fast, the use of phase velocity data in bulk wave model based methods has limitations. First of all, the bulk wave approximations are only valid in a certain frequency range. Indeed, due to the infinite plate assumption in the bulk wave propagation models, the considered wavelength (λ) has to be far smaller than the plate thickness (t), putting a lower boundary on the frequency. At the same time however, the smaller the wavelengths, the more the transmission signals become dominated by the appearance of multiple guided waves in the higher frequency times thick-

ness (fd) regions, thus putting an upper limit on the frequency as well. Additionally, bulk wave based methods typically require a-priori knowledge about the material in terms of symmetry axes, and essentially rely on measurements along these propagation directions. Otherwise, large errors can be encountered in the inverted stiffness parameters [13,14]. As an alternative, the many drawbacks of bulk wave based inversion can be eliminated by considering the full aspects of Lamb wave propagation. Yet, the forward calculation of Lamb wave phase velocities in multilayered composite structures can be hard and may require extreme computational power and time, which increases the complexity of the inversion procedure. Typically, heuristic algorithms, such as the commonly used genetic algorithm [10,11], calls the forward calculation method several thousand times during the global optimization procedure in order to identify all nine stiffness parameters simultaneously. In addition, in order to avoid convergence to a local minimum, the procedure needs to be repeated several times to ensure achieving the global minimum. In the literature, extension of an analytical equivalent single layer thin plate methodology is developed for fast characterization of stiffness and damping at low frequencies (up to 20 kHz) [15]. However, proposed method can only identify up to five stiffness and damping parameters [16].

In the present study, a fast inversion procedure is proposed to characterize the nine orthotropic stiffness parameters of a solid using measured phase velocity information on the first three Lamb modes A_0, S_0 and SH_0 for a plate-like sample. Section 2 of this contribution briefly reviews the basics of the third order shear deformation theory (3SDT), which was selected as the forward model to be embedded in the optimization method based on its accuracy in the low frequency range and its efficiency. The inverse model and the experimental procedure are outlined in Section 3. As a validation of the proposed model, the results for the reconstruction of the stiffness coefficients for an Aluminum plate and a $[45/0/-45/90/-45/0/45/90]_s$ carbon fiber reinforced polymer plate are discussed in Section 4. The results and the performance of the inversion process is evaluated and compared for different heuristic optimization algorithms such as the surrogate optimization, particle swarm optimization, genetic algorithm and simulated annealing. We conclude that the reconstructed stiffness properties for the different optimization approaches compare well with each other and are in excellent agreement with values from literature.

2. FORWARD MODEL

In this section, the expressions for the third order shear deformation theory are derived for an anisotropic composite plate consisting of perfectly bonded layers with constant thickness h. The origin of the coordinate system is located in the center of the plate and it is assumed that the solid material of each layer has a plane of symmetry parallel to the xy plane (see Fig. 1).Additionally, the reflections coming from boundaries are neglected (i.e. the plate is assumed to be infinitely large in X- and Y-directions).

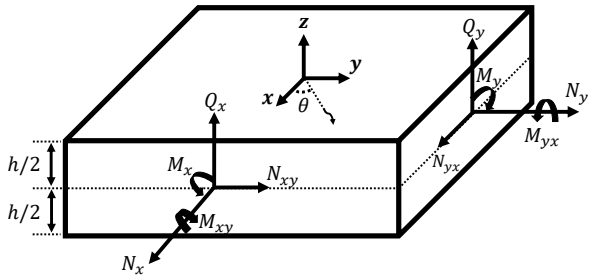

Figure 1. Resultant force and moment identification on a composite plate.

From classical mechanics it is known that when a force is applied to the surface of an object, the body undergoes a small deformation. Following general elasticity, the constitutive relationships for each layer, representing the relation between stresses and strains for an monoclinic material, can be expressed in the following manner

$$\begin{bmatrix} \sigma_x \\ \sigma_y \\ \sigma_z \\ \tau_{yz} \\ \tau_{xz} \\ \tau_{xy} \end{bmatrix} = \begin{bmatrix} C_{11} & C_{12} & C_{13} & 0 & 0 & C_{16} \\ C_{12} & C_{22} & C_{23} & 0 & 0 & C_{26} \\ C_{13} & C_{23} & C_{33} & 0 & 0 & C_{36} \\ 0 & 0 & 0 & C_{44} & C_{45} & 0 \\ 0 & 0 & 0 & C_{45} & C_{55} & 0 \\ C_{16} & C_{26} & C_{36} & 0 & 0 & C_{66} \end{bmatrix} \begin{bmatrix} \varepsilon_x \\ \varepsilon_y \\ \varepsilon_z \\ \gamma_{yz} \\ \gamma_{xz} \\ \gamma_{xy} \end{bmatrix} \tag{1}$$

C_{ij} are the components of the monoclinic stiffness matrix. σ and ε are normal stress and strain values, respectively. Shear stress and strain values are represented by τ and γ, respectively. Although the constitutive relations are belonged to monoclinic materials, the derivations are still valid for the orthotropic materials (subset of monoclinic materials) as well. The amount of strain can be calculated based on the linear strain-displacement relations given in Eq. 2.

$$\begin{aligned} &\varepsilon_x = u_{,x} \qquad \varepsilon_y = v_{,y} \qquad \varepsilon_z = w_{,z} \\ &\gamma_{yz} = v_{,z} + w_{,y} \quad \gamma_{xz} = u_{,z} + w_{,x} \quad \gamma_{xy} = u_{,y} + v_{,x} \end{aligned} \tag{2}$$

where u, v and w are the displacement components in the x, y and z directions, respectively, and partial differentiation is represented by a comma followed by the differentiation variable.

To obtain approximate strain values of the plate, it is common to represent the deformation fields u, v, and w by polynomial functions of a finite degree with respect to the depth variable z, or equivalently as truncated Taylor series in z. The degree of the approximation can be increased to minimize the error of the model, but simultaneously, the complexity of the model and its computational costs will also increase. Besides, for a given level of approximation, the number of computable Lamb wave velocities per frequency equals the number of variables in the displacement

field taken in to account in this approach. Here, in accordance to the 3SDT, the deformation fields are represented as third order polynomials because dispersion curves consisting of 11 lamb wave modes (4 modes from u, 4 modes from v and 3 modes from w) are sufficient for this study.

$$\begin{aligned} u(x,y,z,t) &= u_0(x,y,z,t) + z\psi_x(x,y,z,t) + \\ &\quad z^2\phi_x(x,y,z,t) + z^3X_x(x,y,z,t) \\ v(x,y,z,t) &= v_0(x,y,z,t) + z\psi_y(x,y,z,t) + \\ &\quad z^2\phi_y(x,y,z,t) + z^3X_y(x,y,z,t) + \\ w(x,y,z,t) &= w_0(x,y,z,t) + z\psi_z(x,y,z,t) + \\ &\quad z^2\phi_z(x,y,z,t) \end{aligned} \tag{3}$$

By using Eq. 2 and Eq. 3, the zero, first , second and third order components of the strain values can thus be written in vector notation as

$$\begin{aligned} \varepsilon^{(0)} &= \{u_{0,x}, v_{0,y}, \kappa_3\psi_z, \kappa_2(w_{0,y}+\psi_y), \kappa_1(w_{0,x}+\psi_x), \\ &\quad (u_{0,y}+v_{0,x})\}^T \\ \varepsilon^{(1)} &= \{\psi_{x,x}, \psi_{y,y}, 2\kappa_6\phi_z, \kappa_5(\psi_{z,y}+2\phi_y), \\ &\quad \kappa_4(\psi_{z,x}+2\phi_x), (\psi_{x,y}+\psi_{y,x})\}^T \\ \varepsilon^{(2)} &= \{\phi_{x,x}, \phi_{y,y}, 0, \kappa_8(\phi_{z,y}+3X_y), \kappa_7(\phi_{z,x}+3X_x), \\ &\quad (\phi_{x,y}+\phi_{y,x})\}^T \\ \varepsilon^{(3)} &= \{X_{x,x}, X_{y,y}, 0, 0, 0, (X_{x,y}+X_{y,x})\}^T \end{aligned} \tag{4}$$

To calculate the lamb waves for traction free boundary conditions, σ_z, τ_{yz} and τ_{xz} should be zero. As we work with approximations, the difference between the approximated and actual displacement fields needs to be somehow corrected to obtain these boundary conditions. To eliminate shear correction factors, displacement field can be defined alternative ways [17–19] but it significantly increase the computational power and complexity of the problem. For this reason, shear related terms in Eq. (4) are multiplied with κ_i values.These correction factors $\kappa_i(i$ =1,2,..,8) can be calculated by matching the cut-off frequencies of the A_1, S_1, SH_1 and SH_2 modes in the Lamb wave spectrum based on 3-D elasticity theory [20]. The parameters are derived for isotropic materials but same parameters can also be used for composites with small errors.

$$\begin{aligned} &\kappa_1 = \kappa_2 = \kappa_7 = \kappa_8 = \pi/\sqrt{90 - 2\sqrt{1605}}, \\ &\kappa_3 = \pi/\sqrt{12}, \kappa_4 = \kappa_5 = \kappa_6 = \pi/\sqrt{15}, \end{aligned} \tag{5}$$

Additionally, the resulting stresses and moments per unit length are defined below in the following manner:

$$\begin{aligned} (N_x, N_y, N_z) &= \int_{-h/2}^{h/2} (\sigma_x, \sigma_y, \sigma_z)dz \\ (N_{yz}, N_{xz}, N_{xy}) &= \int_{-h/2}^{h/2} (\tau_{yz}, \tau_{xz}, \tau_{xy})dz \\ (M_x, M_y, M_z) &= \int_{-h/2}^{h/2} (\sigma_x, \sigma_y, \sigma_z)zdz \\ (M_{yz}, M_{xz}, M_{xy}) &= \int_{-h/2}^{h/2} (\tau_{yz}, \tau_{xz}, \tau_{xy})zdz \\ (S_x, S_y, S_z) &= \int_{-h/2}^{h/2} (\sigma_x, \sigma_y, \sigma_z)z^2dz \\ (S_{yz}, S_{xz}, S_{xy}) &= \int_{-h/2}^{h/2} (\tau_{yz}, \tau_{xz}, \tau_{xy})z^2dz \\ (T_x, T_y, T_z) &= \int_{-h/2}^{h/2} (\sigma_x, \sigma_y, \sigma_z)z^3dz \\ (T_{yz}, T_{xz}, T_{xy}) &= \int_{-h/2}^{h/2} (\tau_{yz}, \tau_{xz}, \tau_{xy})z^3dz \end{aligned} \tag{6}$$

With the above definitions, the constitutive equations of a composite laminate with an arbitrary lay-up can be obtained by rearranging Eq. 4 and Eq. 6.

$$\begin{Bmatrix} N \\ M \\ S \\ T \end{Bmatrix} = \begin{bmatrix} [A] & [B] & [D] & [F] \\ [B] & [D] & [F] & [H] \\ [D] & [F] & [H] & [J] \\ [F] & [H] & [J] & [K] \end{bmatrix} \begin{Bmatrix} \varepsilon^{(0)} \\ \varepsilon^{(1)} \\ \varepsilon^{(2)} \\ \varepsilon^{(3)} \end{Bmatrix} \tag{7}$$

where the values of the $ABDFHJK$ matrix correspond to

$$\begin{aligned} &(A_{ij}, B_{ij}, D_{ij}, F_{ij}, H_{ij}, J_{ij}, K_{ij}) = \\ &\quad \int_{-h/2}^{h/2} C_{ij}(1, z, z^2, z^3, z^4, z^5, z^6)dz \end{aligned}$$

Next, by using the principle of virtual displacement (Hamilton's principle), the equations of motion can be calculated [21], i.e., it suffices to require that

$$0 = \int_{t_1}^{t_2} (\delta U + \delta V - \delta K)dt \tag{8}$$

where δU is strain energy, δV is work done by applied force and δK is the kinetic energy. As we expect waves to be traveling in the x and y direction, we can safely assume solutions of the following form:

$$\begin{aligned} \{u_0, v_0, w_0\} &= \{U_0, V_0, W_0\}\text{exp}i[(k_x x + k_y y) - \omega t] \\ \{\psi_x, \psi_y, \psi_z\} &= \{\Psi_x, \Psi_y, \Psi_z\}\text{exp}i[(k_x x + k_y y) - \omega t] \\ \{\phi_x, \phi_y, \phi_z\} &= \{\Phi_x, \Phi_y, \Phi_z\}\text{exp}i[(k_x x + k_y y) - \omega t] \\ \{X_x, X_y\} &= \{x_x, x_y\}\text{exp}i[(k_x x + k_y y) - \omega t] \end{aligned} \tag{9}$$

where ω is the angular frequency, $k_x = k\cos\theta$, $k_y = k\sin\theta$, with k is the wavenumber and θ is propagation direction. In the absence of surface loads, the equations of motion can be rewritten as a generalized eigenvalue problem, with L and I being 11x11 matrices:

$$(L - \omega^2 I)\xi \exp i[k(x\cos\theta + y\sin\theta) - \omega t] = 0 \quad (10)$$

where $\xi = \{U_0 V_0 \Psi_z \Phi_x \Phi_y | W_0 \Psi_x \Psi_y \Phi_z x_x x_y\}^T$. The variables on the left and the right sides of the line relate to the 5 symmetric and 6 antisymmetric modes, respectively, that can be resolved in this approach. Symmetric and antisymmetric modes can be separated if the stacking orientation is symmetric. Details of the method can be found in the literature [20, 22, 23]. By solving the eigenvalue problem given in Eq. 10, phase velocities of 5 symmetric and 6 antisymmetric lamb waves can be calculated in less than a second on a standard laptop. The efficiency and the accuracy of the 3SDT method for low frequency offers the potential to embed this forward model into an inversion algorithm to identify the stiffness parameters based on measured information regarding the low order Lamb modes.

3. INVERSE MODEL

The simultaneous inversion of all components of an orthotropic stiffness matrix demands a substantial amount of computational power because a global optimization algorithm involves the search for the global minimum in a 9 dimensional space (the number of independent stiffness parameters for a orthotropic material). The procedure typically requires thousands of iterations, and many more evaluations of a forward model. Besides, as most of the optimization algorithms are heuristic approaches, the optimization procedure has to be repeated several times to ensure attaining the global minimum. In case of an inefficient forward model, the entire procedure might take days to solve. For this reason, approximated theories, such as the 3SDT explained above, are sometimes better alternatives, especially when the solution time is important. Still, such theories and their embedding in an inversion procedure have to be validated with experimental results. Here, two experimental studies, conducted on different materials and under different circumstances, are considered to validate the proposed 3SDT based inversion method. The first experiment concerns a 5 mm thick Aluminum plate with a density of 2700 kg/m^3. The second experiment deals with a quasi-isotropic (stacking orientation leads in-plane isotropic behavior) composite plate of 2 mm thick and a density of 1571 kg/m^3. The stacking orientation of the composite plate is $[45/0/-45/90/-45/0/45/90]_s$. The data set of the composite plate is open source and can be downloaded from the website given in article [24]. The homogenized stiffness properties for both materials have been reported in the literature [14, 24] and can be found in Table 1.

A broadband (sweep) signal, amplified to 100V, with frequencies ranging from 50 to 200 kHz was supplied to a PZT transducer to excite the aluminum plate. Similarly, a 5 cycle Hanning filtered sine at 240 kHz, amplified to 100 V, was used for the narrowband excitation of the quasi isotropic composite plate. Surface response measurements of the in-plane and out-of-plane velocities were performed with a 3D Infrared Scanning Laser Doppler Vibrometer. The sampling frequencies in the case of aluminum and in the composite case equaled 1.25 MHz and 2.56 MHz, respectively.

Table 1. Literature values of the material properties corresponding to the different materials (in GPa) used in the experiments.

Material	Aluminum	UD134
C_{11}	110.5	56.6
C_{12}	58.5	20.1
C_{13}	58.5	5.7
C_{22}	110.5	56.6
C_{23}	58.5	5.7
C_{33}	110.5	11.0
C_{44}	26.0	3.6
C_{55}	26.0	3.6
C_{66}	26.0	18.2

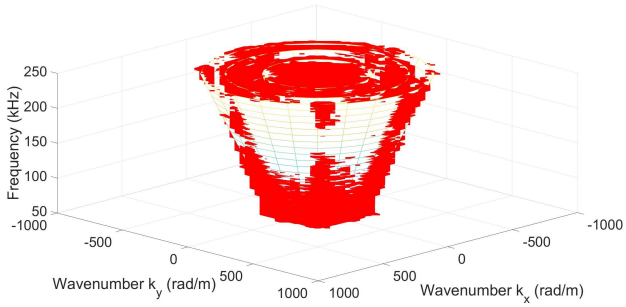

Figure 2. 3D dispersion curves of analytic and experimental results for aluminum.

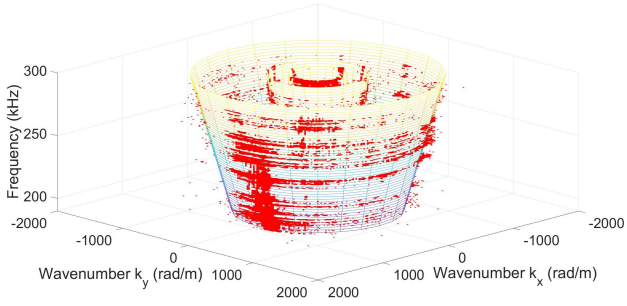

Figure 3. 3D dispersion curves of analytic and experimental results for quasi-isotropic composites.

In preparation of the inversion procedure, the measurement data is converted to the frequency-wavenumber space (k_x, k_y, f) by using 3D Fourier transform. Subsequently,

dispersion surfaces for the A_0, S_0 and SH_0 are extracted in 3D (see Fig. 2 and Fig. 3). Experimental 3D dispersion curves are calculated by using MATLAB™ Image Processing Toolbox. Three levels of threshold has been found for each frequency and images are quantized by using these thresholds. These post-processed data are used as input to the inversion routines. The stiffness tensor components are inverted by maximizing the overlap between the dispersion landscapes of the three measured and the three calculated Lamb wave modes. For this, the cost function to be maximized is built up as the sum of the interpolated values of the post-processed data over the theoretically predicted dispersion surfaces of each mode. The lower boundary and upper boundaries for the C-tensor components are selected as minus 40 and plus 60 percent of the literature values except for C_{33}. As the out of plane stiffness value has a relatively low effect for A_0, S_0 and SH_0 modes, the boundaries of C_{33} are selected as minus 10 and plus 10 percent of the literature value. The optimization is performed by employing four heuristic routines within MATLAB™'s powerful global optimization toolbox, namely genetic algorithm, particle swarm optimization, simulated annealing and surrogate optimization. Each optimization procedure is repeated 100 times to avoid ending up in local minima. The results, along with their statistics, as well as the inversion times for each inversion routine are provided in the next section.

4. RESULTS AND DISCUSSIONS

Statistics of the inverted stiffness matrix results, showing the mean and standard deviation of the optimization results corresponding to the different inversion procedures, can be found in 2 and Table 3 for the aluminum plate and the composite plate, respectively. The relative difference, expressed in percentage, between the obtained median values and the literature values which are assumed to be ground truth values, can be appreciated from Table 4

Comparing the different routines for the aluminum case, it is observed that the particle swarm optimization algorithm provides the best agreement with the values found in the literature, with only 3.1% on average difference. The average difference for the surrogate optimization, simulated annealing and genetic algorithm are 4.6, 4.9 and 6%, respectively. The misfit errors for C_{12}, C_{22} and C_{33} modes for aluminum are relatively higher for all optimization algorithms.

When it comes to the quasi-isotropic composite plate, simulated annealing gives the best fitting results, with a 2.7% difference on average. The average difference for surrogate optimization, particle swarm and genetic algorithm in this case are 4.3, 3.2 and 3.1%, respectively. Note that the misfit error for the C_{13} and C_{23} parameters are again relatively higher indicating that an accurate extraction of the shear stiffness values in the out-of-plane direction is relatively hard to obtain. However, as the four algorithms independently converged to almost the same values in both cases, it is possible that the considered specimens have out-of-plane shear stiffness values that differ from the

Table 2. Statistics of the inverted material properties of an aluminum plate (in GPa) resulting from inversions based on surrogate optimization (SO), particle swarm (PS), simulated annealing (SA) and genetic algorithm (GA). SD stands for standard deviation.

Stiffness	SO Mean - SD	PS Mean - SD
C_{11}	118.6 ± 9.8	113.1 ± 13.4
C_{12}	61.9 ± 6.8	61.6 ± 15.0
C_{13}	60.0 ± 9.1	60.3 ± 11.8
C_{22}	117.3 ± 9.5	119.4 ± 17.5
C_{23}	58.3 ± 7.6	62.2 ± 14.5
C_{33}	116.1 ± 4.8	115.1 ± 4.9
C_{44}	24.4 ± 0.7	25.6 ± 0.9
C_{55}	24.4 ± 1.1	27.1 ± 0.8
C_{66}	26.5 ± 0.5	26.3 ± 0.0
Stiffness	SA Mean - SD	GA Mean - SD
C_{11}	113.7 ± 8.4	114.4 ± 9.1
C_{12}	63.3 ± 7.5	64.7 ± 8.2
C_{13}	60.2 ± 7.7	61.1 ± 7.6
C_{22}	122.9 ± 10.3	125.0 ± 11.7
C_{23}	64.9 ± 8.4	66.9 ± 9.3
C_{33}	111.6 ± 3.4	112.1 ± 4.6
C_{44}	25.3 ± 0.5	25.4 ± 0.6
C_{55}	26.8 ± 0.5	26.9 ± 0.5
C_{66}	26.3 ± 0.2	26.3 ± 0.0

Table 3. Statistics of the inverted material properties of a quasi-isotropic composite plate (in GPa) resulting from inversions based on surrogate optimization (SO), particle swarm (PS), simulated annealing (SA) and genetic algorithm (GA). SD stands for standard deviation.

Stiffness	SO Mean - SD	PS Mean - SD
C_{11}	56.2 ± 1.3	55.3 ± 1.1
C_{12}	21.3 ± 1.3	20.2 ± 1.1
C_{13}	6.5 ± 0.8	6.0 ± 0.9
C_{22}	56.2 ± 1.2	55.3 ± 1.1
C_{23}	6.5 ± 0.8	6.0 ± 0.9
C_{33}	10.7 ± 0.5	11.5 ± 0.5
C_{44}	3.6 ± 0.0	3.6 ± 0.0
C_{55}	3.6 ± 0.0	3.6 ± 0.0
C_{66}	18.6 ± 0.2	18.5 ± 0.3
Stiffness	SA Mean - SD	GA Mean - SD
C_{11}	55.5 ± 0.1	55.2 ± 0.8
C_{12}	20.4 ± 0.1	20.1 ± 0.8
C_{13}	6.2 ± 0.1	6.0 ± 0.6
C_{22}	55.5 ± 0.1	55.2 ± 0.8
C_{23}	6.2 ± 0.1	6.0 ± 0.6
C_{33}	11.1 ± 0.0	11.4 ± 0.4
C_{44}	3.6 ± 0.0	3.6 ± 0.0
C_{55}	3.6 ± 0.0	3.6 ± 0.0
C_{66}	18.2 ± 0.0	18.4 ± 0.2

Table 4. Relative difference, expressed in percentage, for the inverted stiffness components in the case of an aluminum and a quasi-isotropic composite plate with respect to surrogate optimization (SO), particle swarm (PS), simulated annealing (SA) and genetic algorithm (GA).

		Aluminum		
Stiffness	SO	PS	SA	GA
C_{11}	7.8	0.1	2.2	2.6
C_{12}	5.3	1.5	8.2	10.2
C_{13}	5.4	0.1	2.6	3.4
C_{22}	5.6	7.4	11.2	12.7
C_{23}	0.6	6.6	11.9	14.1
C_{33}	6.4	4.5	0.6	0.6
C_{44}	5.6	2.0	2.9	3.0
C_{55}	6.5	4.6	3.5	3.3
C_{66}	1.5	1.0	1.0	1.0
		UD134		
Stiffness	SO	PS	SA	GA
C_{11}	1.0	2.3	2.0	2.0
C_{12}	4.4	0.2	1.1	1.0
C_{13}	13.3	7.8	8.5	8.3
C_{22}	1.0	2.3	2.0	2.0
C_{23}	13.3	7.8	8.5	8.3
C_{33}	2.8	6.2	0.8	4.9
C_{44}	0.8	0.6	0.7	0.6
C_{55}	0.8	0.6	0.7	0.6
C_{66}	1.9	1.3	0.1	0.3

literature values which could be attributed to the manufacturing process. On the other hand, the error percentage is much lower for C_{44}, C_{55} and C_{66} in both cases, and as the standard deviation values for these components in both cases are quite low, it can be clearly concluded that retrieving these stiffness coefficients is easier than finding the others.

The fact that the average error and standard deviation for the aluminum case are higher than for the composite plate inversion might originate from the relatively coarse grid distance and sampling frequency used in the aluminum experiment compared to the composite data. To identify the effect of the sampling frequency and the grid distances, further experiments are required considering different sampling frequencies and grid distances, and the inversion results of each case should be compared to determine the optimum values. Conversely, higher sampling frequencies and lower grid distances increase the measurement time. At the same time, the size of the data used during the inversion also increases which is again crucial for inversion time.

Finally, the average calculation times of the different inversion routines are summarized in Table 5 for one inversion. The reported values correspond to the case of the composite plate, and it was verified that the inversion times approximately scale linearly with the size of the experimental data. In the composite case, the wavenumber grid distance in both axis is 24.5 rad/m from -2000 rad/m to 2000 rad/m, whereas the frequency ranges from 190 kHz to 250 kHz with a 0.625 kHz grid size. Therefore, an experimental data set with a size of 131x131x177 values needs to be loaded at each iteration. Obviously, the inversion time can be reduced by loading a smaller data set but the accuracy might be lowered. The inversion procedure is repeated 100 times (to allow for statistics on the reconstructed values) on a workstation with Intel® Core™ i7-8700 CPU @ 3.20 GHz and 16 GB ram, and the average solution times are shared. The entire model is coded in vectorized form to increase computational efficiency. The solution times for the proposed combination of 3SDT with any of the considered optimization methods show that an acceptably fast and accurate characterization is possible by using this approximate technique.

Table 5. Average solution times (expressed in seconds) for inversions involving surrogate optimization (SO), particle swarm (PS), simulated annealing (SA) and genetic algorithm (GA).

	SO	PS	SA	GA
Time	30.0	410.8	1689.5	1051.5

5. CONCLUSION

An appreciably fast inversion procedure is proposed to identify the stiffness coefficients of an orthotropic composite plate based on experimentally measured Lamb wave phase velocities. The forward model at the heart of the inversion procedure uses a third order shear deformation theory. The investigated heuristic optimization routines include the genetic algorithm, particle swarm optimizer, surrogate optimizer and simulated annealing. To validate the proposed model, experiments on different materials and under different experimental conditions, involving either broadband or narrowband excitation, are conducted. A 3D Infrared Scanning Laser Doppler Vibrometer is used for in-plane and out-of-plane particle velocity measurements. The measured time signal data is converted into frequency-wavenumber space by using 3D Fourier transform from which the dispersion surfaces for the A_0, S_0 and SH_0 modes can be extracted. The resultant dispersion landscapes are then compared with predictions based on the 3SDT. Doing so, orthotropic stiffness tensor components are inferred by minimizing the distance between the measured and calculated lamb wave modes in the 3D wavenumber-frequency space. By using this approximate method, fairly accurate inversions can be completed in acceptable calculation times ranging from 7 to 18 minutes depending on the chosen optimization algorithm. The inverted stiffness properties for both case studies involving an aluminum and quasi-isotropic composite plate are compared with values from the literature, showing a good agreement, with an average misfit error of 3.1% for all 9 stiffness parameters. Stiffness tensor values closest to the

literature are obtained by particle swarm and simulated annealing for the aluminum and the composite plate, respectively. In the end, it can be concluded that the proposed method, combining 3SDT with heuristic optimization routines, allow for a fast and accurate characterization, independent of the considered excitation signals and material symmetry. Unidirectional and cross-ply composite plates as well as layerwise (or individual) stiffness tensor characterization will be examined in future studies.

6. ACKNOWLEDGEMENT

The authors gratefully acknowledge the financial support from the Fund for Scientific Research-Flanders (FWO Vlaanderen, grants G066618N, G0B9515N, 1S45216N and 12T5418N), and the NVIDIA corporation.

7. REFERENCES

[1] J. H. Tam, Z. C. Ong, Z. Ismail, B. C. Ang, and S. Y. Khoo, "Identification of material properties of composite materials using nondestructive vibrational evaluation approaches: A review," *Mechanics of Advanced Materials and Structures*, vol. 24, no. 12, pp. 971–986, 2017.

[2] B. Hosten, M. Deschamps, and B. Tittmann, "Inhomogeneous wave generation and propagation in lossy anisotropic solids. application to the characterization of viscoelastic composite materials," *The Journal of the Acoustical Society of America*, vol. 82, no. 5, pp. 1763–1770, 1987.

[3] S. Rokhlin and W. Wang, "Ultrasonic evaluation of in-plane and out-of-plane elastic properties of composite materials," in *Review of Progress in Quantitative Nondestructive Evaluation*, pp. 1489–1496, Springer, 1989.

[4] B. Hosten, "Elastic characterization of orthotropic composite materials from ultrasonic inspection through non-principal planes," in *Review of progress in quantitative nondestructive evaluation*, pp. 1437–1444, Springer, 1991.

[5] B. Hosten, D. A. Hutchins, and D. W. Schindel, "Air-coupled ultrasonic bulk waves to measure elastic constants in composite materials," in *Review of Progress in Quantitative Nondestructive Evaluation*, pp. 1075–1082, Springer, 1996.

[6] S. Dahmen, H. Ketata, M. H. B. Ghozlen, and B. Hosten, "Elastic constants measurement of anisotropic olivier wood plates using air-coupled transducers generated lamb wave and ultrasonic bulk wave," *Ultrasonics*, vol. 50, no. 4-5, pp. 502–507, 2010.

[7] A. Castellano, P. Foti, A. Fraddosio, S. Marzano, and M. D. Piccioni, "Ultrasonic immersion tests for mechanical characterization of multilayered anisotropic materials," in *2014 IEEE Workshop on Environmental, Energy, and Structural Monitoring Systems Proceedings*, pp. 1–6, IEEE, 2014.

[8] J. Vishnuvardhan, C. Krishnamurthy, and K. Balasubramaniam, "Genetic algorithm reconstruction of orthotropic composite plate elastic constants from a single non-symmetric plane ultrasonic velocity data," *Composites part B: engineering*, vol. 38, no. 2, pp. 216–227, 2007.

[9] M. Sale, P. Rizzo, and A. Marzani, "Semi-analytical formulation for the guided waves-based reconstruction of elastic moduli," *Mechanical Systems and Signal Processing*, vol. 25, no. 6, pp. 2241–2256, 2011.

[10] A. Marzani and L. De Marchi, "Characterization of the elastic moduli in composite plates via dispersive guided waves data and genetic algorithms," *Journal of intelligent material systems and structures*, vol. 24, no. 17, pp. 2135–2147, 2013.

[11] J. Zhao, J. Qiu, and H. Ji, "Reconstruction of the nine stiffness coefficients of composites using a laser generation based imaging method," *Composites Science and Technology*, vol. 126, pp. 27–34, 2016.

[12] S. Rokhlin, D. Chimenti, and P. Nagy, *Physical ultrasonics of composites*. Oxford University Press, 2011.

[13] A. Martens, M. Kersemans, J. Daemen, E. Verboven, W. Van Paepegem, J. Degrieck, S. Delrue, and K. Van Den Abeele, "Numerical study of the time-of-flight pulsed ultrasonic polar scan for the determination of the full elasticity tensor of orthotropic plates," *Composite Structures*, vol. 180, pp. 29–40, 2017.

[14] A. Martens, M. Kersemans, J. Daemen, E. Verboven, W. Van Paepegem, S. Delrue, and K. Van Den Abeele, "Characterization of the orthotropic viscoelastic tensor of composites using the ultrasonic polar scan," *Composite Structures*, vol. 230, p. 111499, 2019.

[15] K. Ege, N. Roozen, Q. Leclère, and R. G. Rinaldi, "Assessment of the apparent bending stiffness and damping of multilayer plates; modelling and experiment," *Journal of sound and vibration*, vol. 426, pp. 129–149, 2018.

[16] F. Marchetti, K. Ege, Q. Leclère, and N. Roozen, "On the structural dynamics of laminated composite plates and sandwich structures; a new perspective on damping identification," *Journal of Sound and Vibration*, p. 115256, 2020.

[17] J. N. Reddy, "A simple higher-order theory for laminated composite plates," 1984.

[18] J. N. Reddy, *Mechanics of laminated composite plates and shells: theory and analysis*. CRC press, 2003.

[19] J. Zhao, H. Ji, and J. Qiu, "Modeling of lamb waves in composites using new third-order plate theories," *Smart materials and structures*, vol. 23, no. 4, p. 045017, 2014.

[20] J. Whitney and C. Sun, "A higher order theory for extensional motion of laminated composites," *Journal of Sound and Vibration*, vol. 30, no. 1, pp. 85–97, 1973.

[21] K. Washizu, *Variational methods in elasticity and plasticity*, vol. 3. Pergamon press Oxford, 1975.

[22] L. Wang and F. Yuan, "Lamb wave propagation in composite laminates using a higher-order plate theory," in *Nondestructive Characterization for Composite Materials, Aerospace Engineering, Civil Infrastructure, and Homeland Security 2007*, vol. 6531, p. 65310I, International Society for Optics and Photonics, 2007.

[23] M. A. Torres-Arredondo and C.-P. Fritzen, "A viscoelastic plate theory for the fast modelling of lamb wave solutions in ndt/shm applications," *Ultragarsas" Ultrasound"*, vol. 66, no. 2, pp. 7–13, 2011.

[24] J. Moll, J. Kathol, C.-P. Fritzen, M. Moix-Bonet, M. Rennoch, M. Koerdt, A. S. Herrmann, M. G. Sause, and M. Bach, "Open guided waves: online platform for ultrasonic guided wave measurements," *Structural Health Monitoring*, vol. 18, no. 5-6, pp. 1903–1914, 2019.